Effect of cryogenic temperature and change of strain path on grain refinement during rolling of Cu–30Zn brass

T. Konkova[a], S. Mironov[a,b], A. Korznikov[a,c], G. Korznikova[a], M.M. Myshlyaev[d], S.L. Semiatin

[a]Institute for Metals Superplasticity Problems, Russian Academy of Science, Ufa 450001, Russia
[b]Institute for Metals Superplasticity Problems, Russian Academy of Science, Ufa 450001, Russia; and Department of Materials Processing, Graduate School of Engineering, Tohoku University, Sendai 980-8579, Japan
[c]National Research Tomsk State University, Tomsk 634050, Russia
[d]Baikov Institute of Metallurgy and Material Science, Russian Academy of Science, Moscow 119991, Russia; and Institute of Solid State Physics, Russian Academy of Sciences, Chernogolovka, Moscow oblast 142432, Russia
[e]Air Force Research Laboratory, Materials and Manufacturing Directorate, AFRL/RXCM, Wright-Patterson AFB, Ohio 45433-7817, USA

The effect of cryogenic temperature and change of strain path on grain refinement during the rolling of Cu–30Zn brass was determined. To this end, the material was unidirectionally rolled or cross-rolled to 90% thickness reduction at either ambient or liquid-nitrogen temperatures, and the resulting grain structures and crystallographic textures were determined via electron backscatter diffraction (EBSD) technique. In all cases, grain refinement was found to be governed primarily by twinning and shear banding. Lowering of the rolling temperature to the cryogenic range was found to provide only a minor effect. Cryogenic rolling was thus concluded to impart no practical benefit with regard to grain refinement or property improvement for this material. In contrast, a change of strain path via cross rolling was shown to enhance twinning and shear banding and thus to promote the formation of a relatively homogeneous ultrafine-grain microstructure.

Keywords:

Cu–30Zn brass
Grain refinement
Cryogenic deformation
Change of strain path
Electron backscatter diffraction
Grain structure

1. Introduction

A large deformation at cryogenic temperatures is sometimes considered as a promising and cost-effective method for producing bulk ultrafine-grain materials [1–15]. However, recent detailed microstructural observations of cryo-deformed aluminum and copper have revealed no significant grain-

refinement effect [1,2]. This disappointing finding has been related with a retardation of the formation of dislocation boundaries due to the suppression of cross-slip under cryogenic conditions [2]. On the other hand, pronounced microstructural refinement has been found during cryogenic deformation of commercial-purity titanium [3] and alpha brass [4,7] and has been attributed to extensive mechanical twinning and shear banding. From these observations, cryogenic deformation was concluded to be particularly effective for the materials prone to activation of these two deformation mechanisms.

Recent work [8] has demonstrated that grain-structure evolution and texture development during cryogenic rolling of Cu–30Zn brass are broadly similar to those during conventional (room-temperature) cold rolling [16]. Specifically, profuse mechanical twinning is observed, but it occurs very heterogeneously. Due to variations in the Schmid factor, the twins are concentrated preferentially in grains with orientations close to copper {112}<111> and S {123}<634>, whereas Goss {110}<100> and Brass {110}<112> grains are typically twin-free. The twinned areas subsequently undergo extensive shear banding which promote the formation of an ultrafine-grain structure. On the other hand, the twin-resistant Goss and Brass orientations exhibit only limited grain refinement. As a result, the microstructure so produced is extremely inhomogeneous, consisting of millimeter-scale remnants of original grains and ultrafine-grain domains.

Considering the above similarities of microstructure evolution during cryogenic and conventional cold rolling, a possible benefit of cryogenic deformation for grain refinement in Cu–30Zn brass is not evident. To clarify this issue, the present work was undertaken to provide a direct comparison of the microstructures obtained after comparable strains under ambient and cryogenic conditions. Furthermore, it may be hypothesized that the refinement of "stagnant" Goss and Brass orientations during rolling may be stimulated by a change in strain path. For instance, a change of the rolling direction may activate mechanical twinning and shear banding in these grains and thus promote the formation of a more-uniform ultrafine-grain microstructure. To examine this idea, the grain refinement efficiency of unidirectional and cross-rolling was also established in the present work.

2. Materials and methods

The program material comprised Cu–30Zn, variously referred to as yellow or cartridge brass, with a measured composition (in wt.%) of 29.5 Zn, 0.5 Pb, and balance Cu. It was manufactured by ingot casting followed by 10 pct. cold rolling and subsequent annealing at 800 °C for 30 min. This processing route produced millimeter-size grains with a significant fraction of retained original dendritic structure.

The material was rolled to 90% overall thickness reduction (true strain = −2.3) at either ambient or cryogenic temperature using either unidirectional or cross-rolling. To ensure a homogeneous strain distribution during rolling, a relatively low reduction per pass of 10 pct. was used. Cross-rolling comprised a 90° rotation between each passes. In order to ensure cryogenic deformation conditions, the rolling perform and work rolls were soaked in liquid nitrogen prior to each pass and held for 20 min; immediately after each pass, the workpiece was re-inserted into liquid nitrogen. The typical flat-rolling

convention was adopted in this work; i.e. the rolling, long-transverse, and thickness/normal directions were denoted as RD, TD, and ND, respectively.

To provide in-depth insight into deformation-induced microstructures, characterization was performed primarily by an electron backscatter diffraction (EBSD) technique. In all cases, the mid-thickness rolling plane (containing the RD and TD) was examined. For microstructural observations, samples were prepared using conventional metallographic techniques followed by long-term (24 h) vibratory polishing with a colloidal-silica suspension. EBSD analysis was conducted with a JSM-7800F field-emission-gun, scanning-electron microscope equipped with a TSL OIM™ EBSD system. To examine microstructure at different scales, several EBSD maps were acquired from each rolled sample using a scan step size of 0.05 or 0.25 μm. To differentiate the maps, they are denoted as "high-resolution" and "low resolution", respectively, throughout this paper. To improve the reliability of the EBSD data, small grains comprising three or fewer pixels were automatically removed from the maps using the grain-dilation option in the TSL software. Furthermore, to eliminate spurious boundaries caused by orientation noise, a lower limit boundary misorientation cutoff of 2° was used. A 15° criterion was employed to differentiate low-angle boundaries (LABs) and high-angle boundaries (HABs). Grain size was quantified by the determination of the area of each grain and the calculation of its circle-equivalent diameter, i.e., the so-called grain reconstruction method was applied [17].

To obtain a broader view of the deformation-induced microstructures, the Vickers microhardness was also measured on each sample at ambient temperature using a load of 100 g for 10 s. For this purpose, 25 measurements were made in each case to obtain an average value.

Because of the very large initial grain size, there was substantial variation in the deformed microstructures throughout the samples. This made quantitative evaluation of the typical microstructure and texture parameters difficult, and, consequently, qualitative microstructure and texture trends are presented in this paper.

3. Results

3.1. Broad aspects of deformation-induced microstructures

For preliminary evaluation of the grain-refinement efficiency of different rolling conditions and to provide broad insight into microstructure evolution, the microhardness of the initial and rolled materials was measured (Fig. 1). These results indicated that the material strength was almost tripled during rolling. On the other hand, all rolled specimens exhibited nearly the same microhardness level with the difference typically being within experimental scatter. This finding suggested a similarity in microstructure for each material condition that was investigated. In addition, the material rolled at ambient temperature showed relatively large experimental scatter, thus indirectly suggesting a high degree of microstructure heterogeneity.

The deformation-induced microstructures at a relatively coarse scale were apparent in low-resolution inverse-pole figure (IPF) EBSD orientation maps taken from the rolled materials (Fig. 2). In these maps, individual grains were colored according to their crystallographic directions relative to the ND using the

typical color-code triangle (shown in the bottom right corner). From a broad perspective, the microstructures of both unidirectionally rolled specimens (Figs. 2a and b) consisted of bands aligned with the RD and having a crystallographic orientation close to <110>//ND or <111>//ND (green and blue colors, respectively). In each of the cross-rolled specimens (Figs. 2c and d), the microstructure was more complex, but some evidence of similar texture bands were also evident.

More detailed information on crystallographic orientations was obtained from orientation distribution functions (ODFs) derived from the EBSD data (Fig. 3); for simplicity, only $\varphi 2 = 0°$ and $\varphi 2 = 45°$ ODF sections are shown in the figure. For comparison purposes, several ideal rolling orientations for face-centered-cubic metals (after Hirsch, et al. [16]) are also indicated. To a first approximation, the textures in all rolled conditions could be interpreted in terms of the superposition of the Brass {110}<112> and Goss {110}<100> components and typically also include the Y {111}<112> orientation (Fig. 3). Therefore, the green and blue texture bands in the EBSD maps in Fig. 2 consisted of brass/Goss and Y orientations, respectively.

In both cross-rolled specimens, the textures were relatively weak and more diffuse presumably due to the change in strain path. Despite the presence of experimental scatter (which was presumably related with the limited statistics of the measurements, as described in Section 2), the textures in each of the rolled conditions appeared to be fundamentally similar. In all cases, they were as expected for heavily cold-rolled Cu–30Zn brass [16]; specifically, the Brass component is commonly accepted to be the stable end orientation, whereas Y and Goss are typically transient orientations originating from twinning, slip, and subsequent shear banding [16]. The origin of the latter two orientations is discussed in more detail in Sections 4.2 and 4.3.

Further insight into microstructure evolution was obtained from EBSD grain-boundary and Kikuchi-band-contrast maps (Figs. 4 and 5, respectively). From the grain-boundary maps (Fig. 4), it appeared that the grain structures developed in all rolled conditions were also largely similar to each other and could be described in terms of a mixture of coarse remnants of the original grains, twins, and ultra-fine-grain domains. From comparison with the orientation maps in Fig. 2, it is evident that crystallographic orientations of the coarse-grain remnants were close to the Brass and Goss components, whereas the twinned and ultrafine-grain areas were often concentrated within the Y orientation. The material unidirectionally rolled at cryogenic temperature (Fig. 4b) as well as both cross-rolled specimens (Figs. 4c and d) seemed to contain a larger fraction of ultrafine grains and a denser LAB substructure.

The EBSD results (Fig. 4) were further amplified by Kikuchi-band contrast maps which exhibited numerous dark bands (Fig. 5) which were associated almost exclusively with the ultrafine-grain domains. Thus, these domains can be interpreted as shear bands which are typically observed in heavily cold-rolled brass [16]. The shear banding was more pronounced in the cross-rolled materials (Fig. 5).

3.2. High-resolution microstructure observations

As shown in the previous section, the microstructures in all rolled conditions consisted of coarse remnants of the original grains intermixed with twins and ultrafine-grain domains. To provide a clearer

view of the substructure developed within these microstructural constituents, high resolution maps were taken from appropriate regions (Figs. 6 and 7).

In the relatively coarse-grain areas, the substructure typically contained nearly parallel arrays of LABs which were more or less aligned with traces of {111}-planes (Fig. 6). In the unidirectionally rolled specimens, these LAB arrays were a dominant microstructural element (Figs. 6a and b). Such lamellar substructures are typical for heavily cold-rolled cubic metals, and are usually attributed to the activation of a grain-subdivision mechanism [18]. The observed lamellar boundaries were typically low-angle in nature, and high-angle segments were rarely observed (Fig. 6). This indicated perhaps that the kinetics of the LAB-to-HAB transformation were relatively slow; i.e. the normal grain subdivision process was sluggish. Considering the low stacking fault energy of the program material as well as the low deformation temperature (for cryo-rolled specimens), this result seems to be as expected.

In addition to the lamellar substructure, the coarse-grain areas also contained mechanical twins and sporadic shear bands (examples are indicated with arrows in Fig. 6). The latter two microstructural elements were much more pronounced in both cross-rolled conditions (Figs. 6c and d). This observation is discussed in more detail in Sections 4.2 and 4.3.

The high-resolution EBSD grain-boundary maps of the ultrafine grain regions are summarized in Fig. 7. In all cases, the microstructures were dominated by ~0.2 μm grains with a low-aspect ratio (within the shear bands) but also included twins and a high density of LABs. All microstructures were broadly similar to each other, thus indicating that the grain refinement was basically the same in all rolling conditions being largely a result of shear banding and mechanical twinning.

4. Discussion

4.1. Coarse remnant grains

As mentioned in the introduction, the presence of coarse remnants of original grains is one of the key problems of grain refinement during cryo-rolling of Cu–30Zn brass. Fig. 4 provided evidence that this problem is more or less inherent to all of the rolling conditions investigated herein. To ascertain the "stagnant" nature of retained coarse grains, their specific crystallographic orientations were determined and quantified in ODFs (Fig. 8). Each of these orientation distributions was characterized by the predominance of a strong brass orientation and typically contained the Goss texture component. For unidirectional rolling, these two orientations are well known to have a low ratio of the twinning-to-slip Schmid-factors (0.77 and 0.55, respectively) [16]. Accordingly, almost no twinning occurred in these grains, and thus grain refinement was essentially inhibited. Due to the crystallographic nature of twinning, therefore, simply lowering the rolling temperature to the cryogenic range is not sufficient for activation of this mechanism in the "stagnant" grains and thus to promote their refinement.

As follows from Figs. 4c and d, this trend was also observed for crossrolling, although it was less pronounced, as is discussed further below.

4.2. Twinning

Due to the large impact of twinning and shear banding on grain refinement in all rolled conditions, their origin was of particular interest.

Thus, the crystallographic aspects of these microstructural features are considered in the following two sections.

To provide fundamental insight into the twinning occurring in each rolling sequence, the crystallographic orientations of the twinned areas were also extracted from EBSD maps and plotted as ODFs (Fig. 9). In both unidirectionally rolled conditions, the orientation distributions were dominated by a pronounced Y-texture component (Figs. 9a and b). This observation was as expected for heavily cold-rolled brass. The Y texture is commonly accepted to originate from mechanical twinning of grains with a copper {112}<111> orientation, which occurs at an intermediate level of rolling reduction, and the subsequent slip of the twinned and matrix material on the common {111} twinning plane [16]. The broad similarity in crystallography of the twinned areas in both unidirectionally rolled conditions suggests that the twinning mechanism was essentially the same at ambient and cryogenic temperatures.

During cross-rolling, however, this process was somewhat different. In addition to the Y orientation, the ODF for cross-rolled specimens also contained brass and Goss components (Figs. 9c and d). As mentioned in the previous section, for unidirectional rolling these orientations are well accepted to be stable against twinning due to a relatively low Schmid factor. However, a change of strain path during cross rolling promotes twinning even in such grains (Figs. 6c and d) and thus improves microstructure homogeneity.

To provide additional insight into the twinning process, the twin boundary-area per unit volume was also quantified. To this end, misorientation-angle distributions were derived from the twinned areas and are summarized in Fig. 10. These plots indicated that neither the lowering of the rolling temperature to the cryogenic range nor a change in strain path increased the twin-induced peak (at a misorientation angle of 60°). This means perhaps that changes in rolling conditions did not substantially reduce the twin size. On the other hand, cross rolling increased the angular spread around the twin-induced peak (indicated by the arrow in Fig. 10). This trend can be attributed to the deviation of the twin-boundary misorientation from the exact twin-matrix relationship due to crystallographic slip and rotation of the twins and matrix during subsequent strain. The enhancement of this process during cross-rolling may be related to the more pronounced shear banding.

Cryogenic rolling as well as a change in strain path also promoted a significant increase of LAB area in the twinned regions (Fig. 10).

4.3. Shear banding

To a first approximation, the ODFs for the shear bands developed in both unidirectionally rolled specimens (Figs. 11a and b) could be described primarily in terms of the superposition of Y, Goss, and Brass orientations. Again, this is in line with the well-accepted understanding of shear band development during cold rolling of Cu–30Zn brass [16]. As mentioned above, the Y orientation originates from twinning of copper texture components followed by slip. After achieving the Y orientation, subsequent slip is believed to become increasingly difficult because the Schmid factor for the activated system decreases towards zero. This gives rise to shear banding to accommodate further imposed deformation

leading to a rotation of the Y orientation towards the Goss orientation. Subsequent slip in the Goss component produces the final stable Brass texture. Thus, the presence of Y, Goss, and Brass orientations within the shear bands revealed in the present work reflected different stages of texture development within these zones. The broad similarity of the ODFs in Figs. 11a and b indicates that the shear banding mechanism was largely the same at ambient and cryogenic temperatures.

In the cross-rolled material, extensive shear banding was also observed in the stable Goss and Brass orientations (Figs. 6c, d and 11c). This was likely related to the change in strain path, but the exact microstructural mechanism is not clear. Similar to twinning, the shear banding promoted refinement of these "stable" orientations, thus improving global microstructure uniformity. The somewhat specific characteristic of shear banding during cross-rolling was also supported by misorientation measurements (Fig. 12a), which revealed an increased proportion of twin boundaries within the shear bands. On the other hand, grain-size distributions within the shear bands were nearly the same for all rolling conditions (Fig. 12b); the mean grain size was ~0.2 μm.

Considering the observed differences in microstructure, the nearly similar microhardness values found for all of the rolled conditions (Fig. 1) may seem surprising. Nevertheless, it should be borne in mind that the strength of low-stacking-fault-energy materials (including Cu–30Zn brass) at ambient temperature is believed to be heavily influenced by work hardening. Therefore, the observed insensitivity of the hardness of the deformed materials to variations in grain structure likely indicates similar dislocation density for each of the rolling conditions that were investigated.

5. Conclusions

The effect of cryogenic temperature and a change in strain path on grain refinement during rolling of Cu–30Zn brass was investigated. To this end, samples were unidirectionally or cross-rolled to 90% thickness reduction at either ambient or liquid-nitrogen temperatures, and the resulting grain structures and crystallographic textures were determined via high-resolution EBSD. The room-temperature microhardness was also measured for both rolling conditions.

In all cases, grain refinement was found to be governed primarily by twinning and shear banding. Normal grain subdivision processes involving gradual LAB-to-HAB transformation were deduced to be sluggish.

A lowering of the rolling temperature to the cryogenic range was found to provide only a minor effect. It seems therefore that cryogenic rolling has no practical benefit for grain refinement in Cu–30Zn brass. Furthermore, unidirectional rolling at ambient as well as cryogenic temperatures produced an extremely inhomogeneous microstructure consisting of millimeter-scale remnants of original grains having stable crystallographic orientations and ultrafine-grain domains.

A change of strain path via cross rolling was shown to enhance twinning and shear banding in the stable rolling orientations, thus promoting the formation of a more uniform ultrafine-grain microstructure.

Acknowledgments

Financial support from the Russian Fund of Fundamental Research (project No.14-02-97004) is gratefully acknowledged. The authors are grateful to P. Klassman for technical assistance during cryogenic rolling.

References

[1] Y. Huang, P.B. Prangnell, The effect of cryogenic temperature and change in deformation mode on the limiting grain size in a severely deformed dilute aluminium alloy, Acta Mater. 56 (2008) 1619–1632.

[2] T. Konkova, S. Mironov, A. Korznikov, S.L. Semiatin, Microstructural response of pure copper to cryogenic rolling, Acta Mater. 58 (2010) 5262–5273.

[3] S.V. Zherebtsov, G.S. Dyakonov, A.A. Salem, V.I. Sokolenko, G.A. Salishchev, S.L. Semiatin, Formation of nanostructures in commercial-purity titanium via cryorolling, Acta Mater. 61 (2013) 1167–1178.

[4] G.H. Xiao, N.R. Tao, K. Lu, Microstructures and mechanical properties of a Cu–Zn alloy subjected to cryogenic dynamic plastic deformation, Mater. Sci. Eng. A 513–514 (2009) 13–21.

[5] Y.S. Li, N.R. Tao, K. Lu, Microstructural evolution and nanostructure formation in copper during dynamic plastic deformation at cryogenic temperatures, Acta Mater. 56 (2008) 230–241.

[6] Y. Zhang, N.R. Tao, K. Lu, Mechanical properties and rolling behaviors of nanograined copper with embedded nano-twin bundles, Acta Mater. 56 (2008) 2429–2440.

[7] J. Das, Evolution of nanostructure in α-brass upon cryorolling, Mater. Sci. Eng. A 530 (2011) 675–679.

[8] T. Konkova, S. Mironov, A.V. Korznikov, G. Korznikova, M.M. Myshlyaev, S.L. Semiatin, Grain structure evolution during cryogenic rolling of alpha brass, J. Alloys Compd. 629 (2015) 140–147.

[9] S.K. Panigrahi, R. Jayaganathan, A study on the mechanical properties of cryorolled Al–Mg–Si alloy, Mater. Sci. Eng. A 480 (2008) 299–305.

[10] A. Kauffmann, J. Freudenberger, H. Klaub, W. Schilinger, V. Subramanya Sarma, L. Schultz, Efficiency of the refinement by deformation twinning in wire drawn single phase copper alloys, Mater. Sci. Eng. A 624 (2015) 71–78.

[11] V. Subramanya Sarma, J. Wang, W.W. Jian, A. Kauffmann, H. Conrad, J. Freudenberger, Y.T. Zhu, Role of stacking fault energy in strengthening due to cryo-deformation of FCC metals, Mater. Sci. Eng. A 527 (2010) 7624–7630.

[12] K.P. Sushanta, R. Jayaganathan, A study of the mechanical properties of cryorolled Al–Mg–Si alloy, Mater. Sci. Eng. A 480 (2008) 299–305.

[13] V. Subramanya Sarma, K. Sivaprasad, D. Sturm, M. Heilmaier, Microstructure and mechanical properties of ultra fine grained Cu–Zn and Cu–Al alloys produced by cryorolling and annealing, Mater. Sci. Eng. A 489 (2008) 253–258.

[14] K. Edalati, J.M. Cubero-Sesin, A. Alhamidi, I.F. Mohamed, Z. Horita, Influence of severe plastic deformation at cryogenic temperature on grain refinement and softening of pure metals: investigation using high-pressure torsion, Mater. Sci. Eng. A 613 (2014) 103–110.

[15] K.C. Sekhar, R. Narayanasamy, K. Velmanirajan, Experimental investigations on microstructure and formability of cryorolled AA 5052 sheets, Mater. Des. 53 (2014) 1064–1070.

[16] J. Hirsch, K. Lucke, M. Hatherly, Mechanism of deformation and development of rolling textures in polycrystalline F.C.C. metals: III. The influence of slip inhomogeneities and twinning, Acta Metall. 36 (1988) 2905–2927.

[17] F.J. Humphreys, Quantitative metallography by electron backscatter diffraction, J. Microsc. 195 (1999) 170–185.

[18] N. Hansen, D.J. Jensen, Development of microstructure in FCC metals during cold work, Philos. Trans. Soc. Lond. A 357 (1999) 1447–1469.

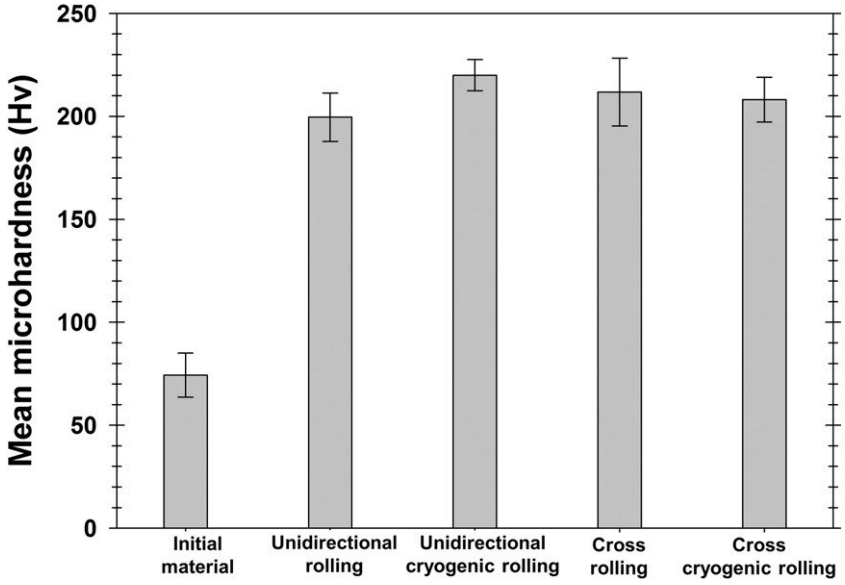

Fig. 1. Effect of cryogenic temperature and change in rolling direction on microhardness. Error bars indicate the standard deviations for the measurements. In all cases, the microhardness was measured at ambient temperature.

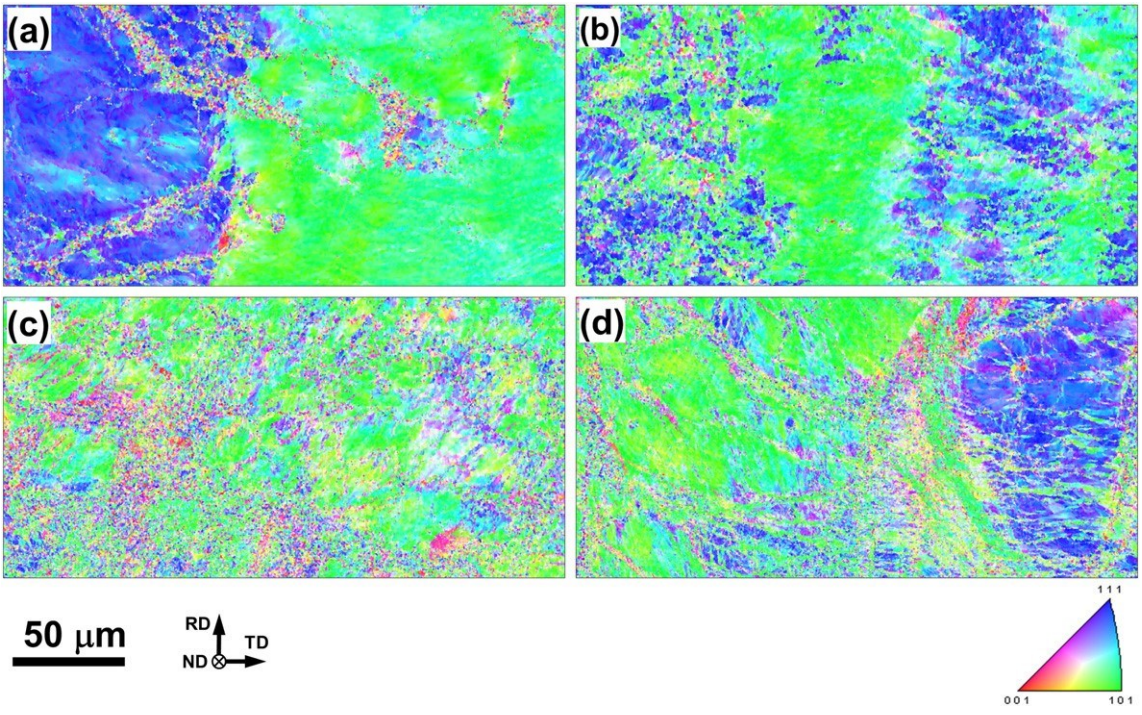

Fig. 2. Selected portions of low resolution EBSD orientation maps illustrating the microstructure developed during (a) unidirectional rolling at room temperature, (b) unidirectional rolling at cryogenic temperature, (c) cross-rolling at room temperature, and (d) cross-rolling at cryogenic temperature. In the maps, the colors indicate the variation in crystallographic orientation relative to the ND; the color code triangle is given in the bottom right corner.

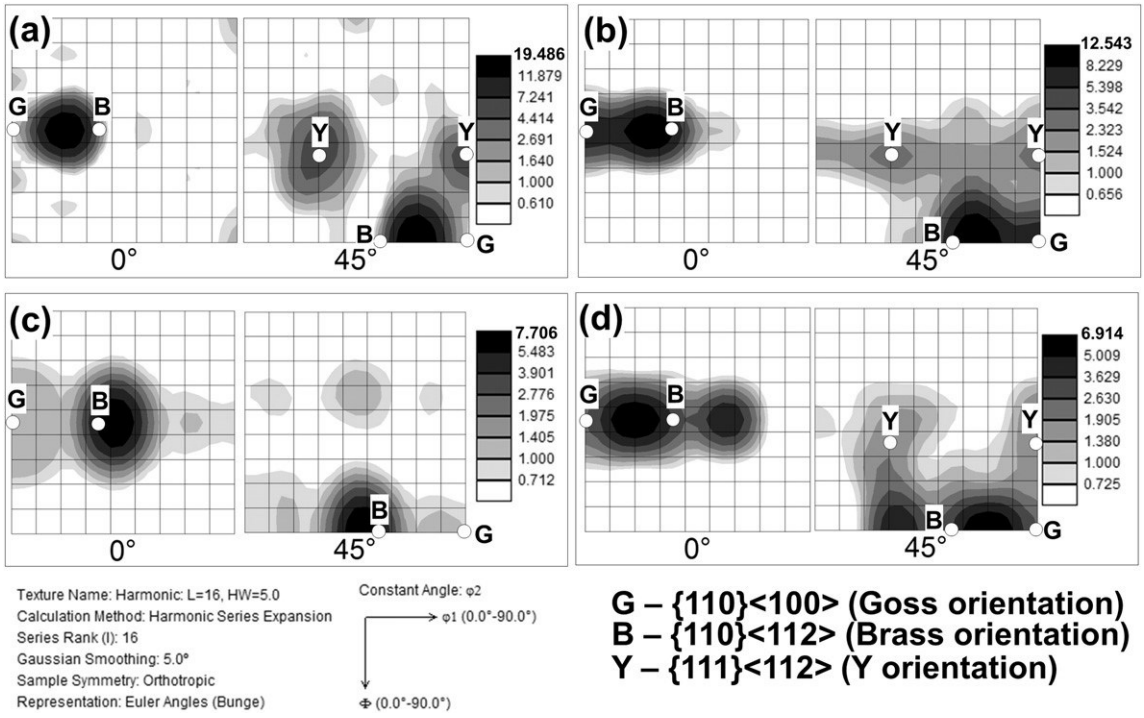

Fig. 3. φ2 = 0° and φ2 = 45° sections of orientation-distribution functions (ODFs) for material which was (a) unidirectionally rolled at room temperature, (b) unidirectionally rolled at cryogenic temperature, (c) cross-rolled at room temperature, and (d) cross-rolled at cryogenic temperature. For comparison purposes, several ideal rolling orientations are superimposed on the ODFs.

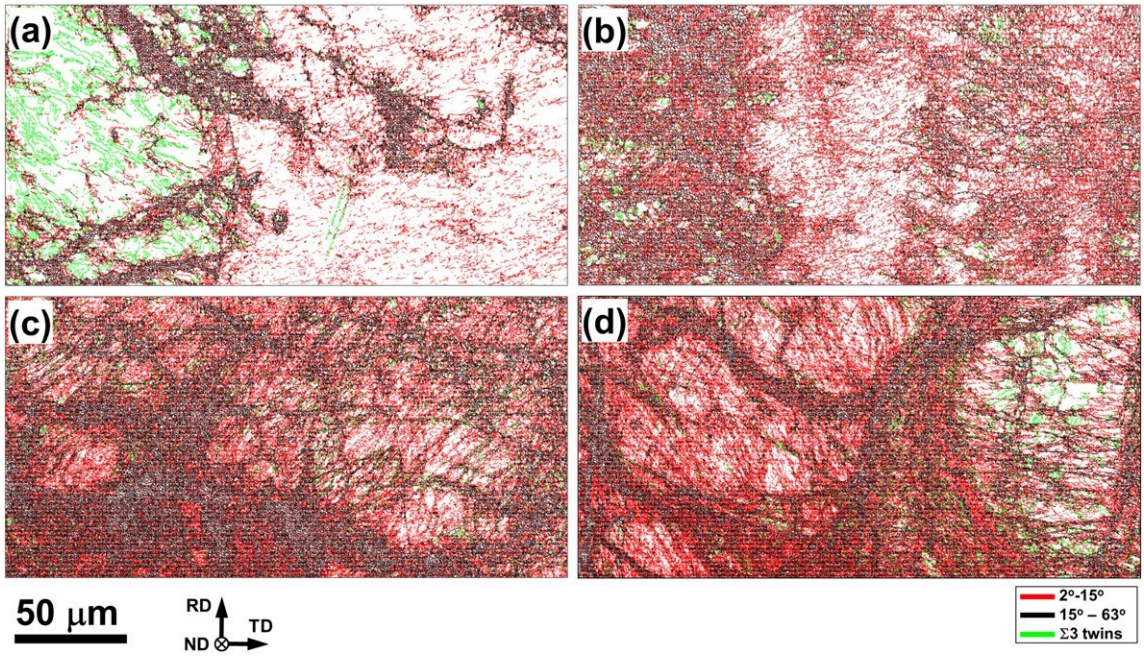

Fig. 4. Selected portions of low-resolution EBSD grain-boundary maps illustrating the microstructure developed during (a) unidirectional rolling at room temperature, (b) unidirectional rolling at cryogenic temperature, (c) cross-rolling at room temperature, and (d) cross-rolling at cryogenic temperature. In the grain-boundary maps, misorientation levels are given in the bottom right corner.

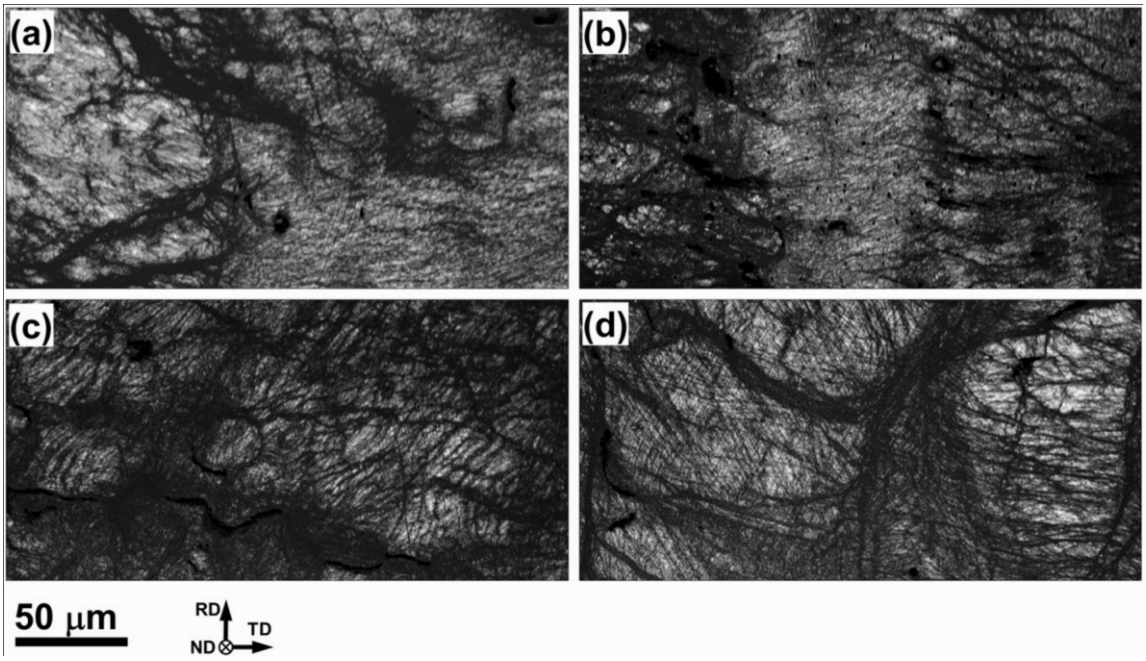

Fig. 5. Selected portions of low-resolution EBSD Kikuchi-band-contrast maps illustrating the microstructure developed during (a) unidirectional rolling at room temperature, (b) unidirectional rolling at cryogenic temperature, (c) cross-rolling at room temperature, and (d) cross-rolling at cryogenic temperature. In the maps, the dark bands are shear bands.

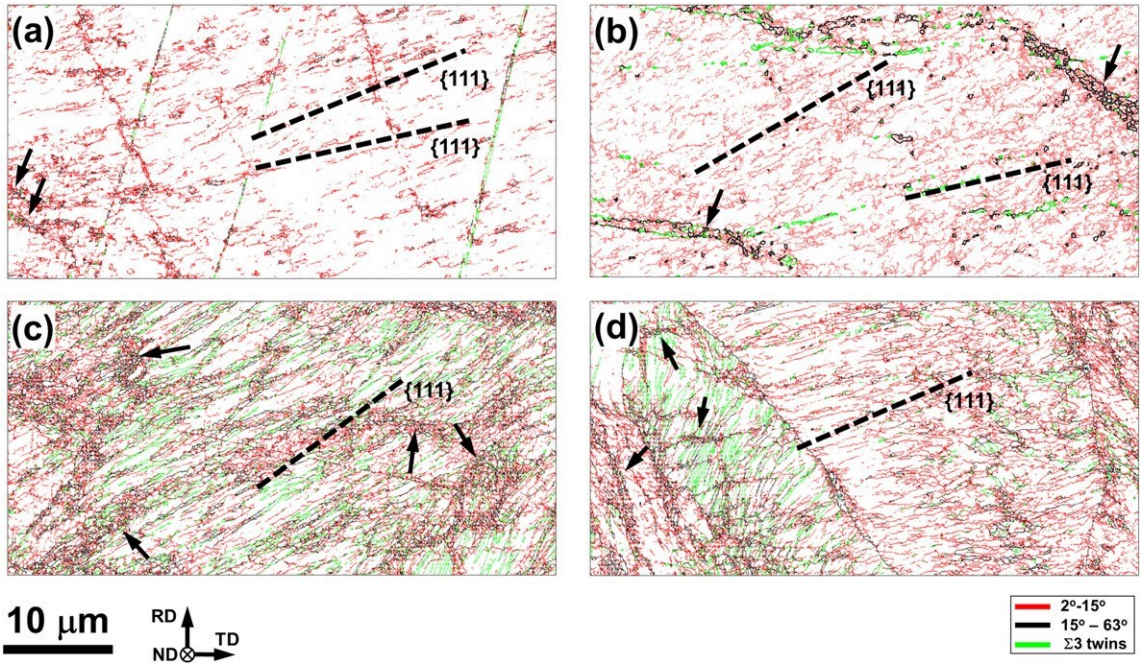

Fig. 6. Selected portions of high-resolution EBSD grain-boundary maps illustrating the substructure within relatively coarse-grained areas in the material developed during (a) unidirectional rolling at room temperature, (b) unidirectional rolling at cryogenic temperature, (c) cross-rolling at room temperature, and (d) cross-rolling at cryogenic temperature. In the grain-boundary maps, misorientation levels are given in the bottom right corner. Broken lines show the orientations of {111} plane traces closest to the deformation-induced boundaries. Arrows indicate shear bands.

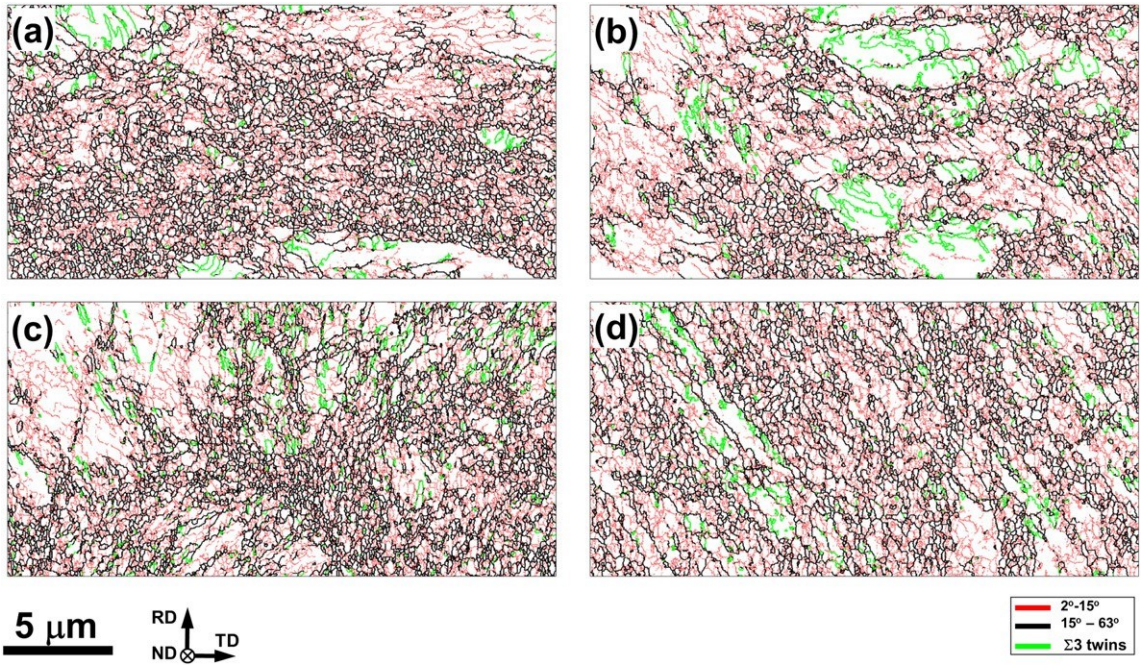

Fig. 7. Selected portions of high-resolution EBSD grain-boundary maps illustrating ultrafine-grain domains developed during (a) unidirectional rolling at room temperature, (b) unidirectional rolling at cryogenic temperature, (c) cross-rolling at room temperature, and (d) cross-rolling at cryogenic temperature. In the grain-boundary maps, the misorientation levels are given in the bottom right corner.

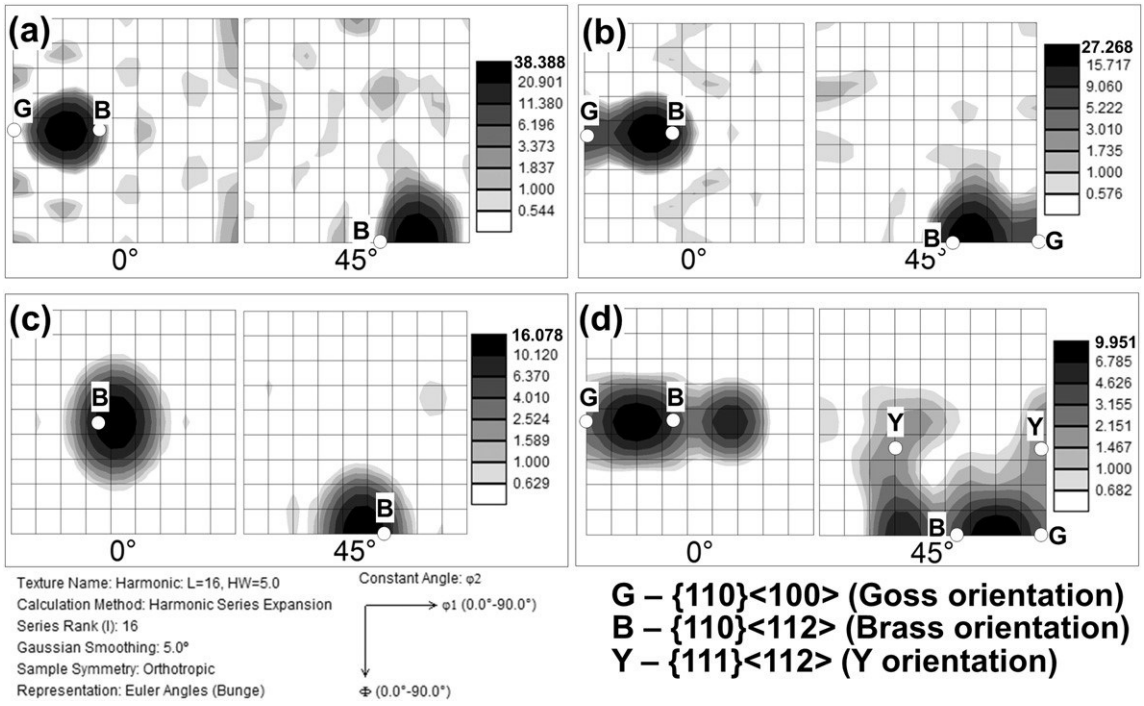

Fig. 8. φ2 = 0° and φ2 = 45° sections of ODFs for the coarse remnants of original grains within the material which was (a) unidirectionally rolled at room temperature, (b) unidirectionally rolled at cryogenic temperature, (c) cross-rolled at room temperature, and (d) cross-rolled at cryogenic temperature. For comparison purposes, several ideal rolling orientations are superimposed on the ODFs.

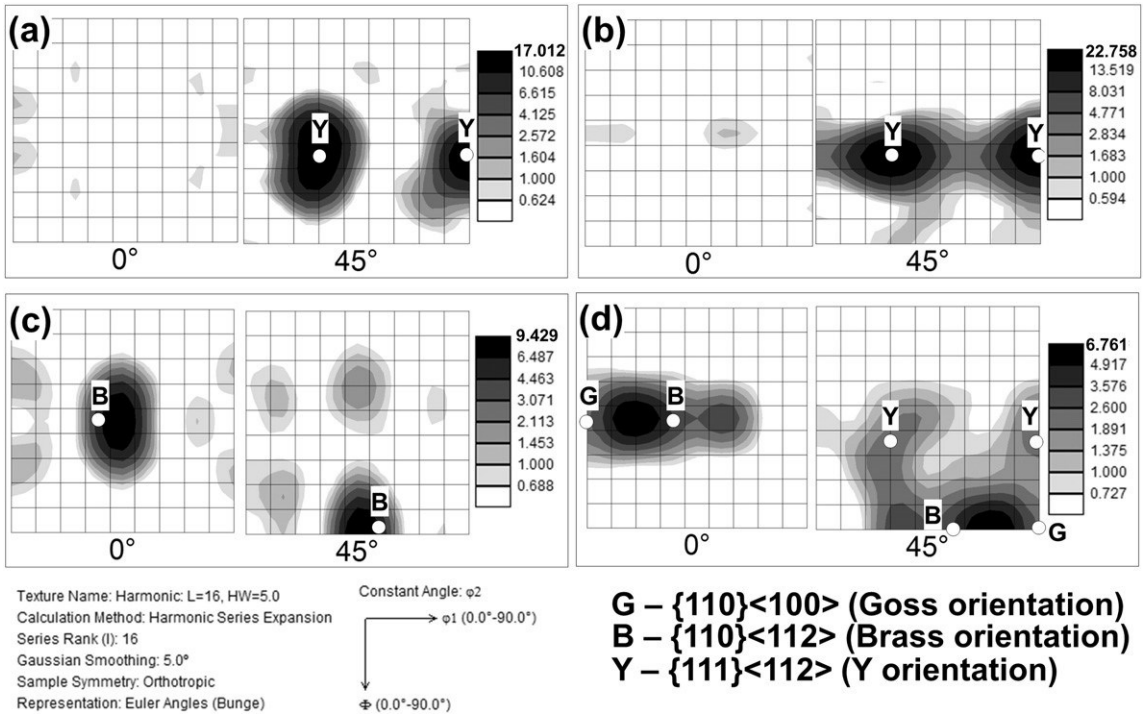

Fig. 9. φ2 = 0° and φ2 = 45° sections of orientation-distribution functions (ODFs) for twinned areas developed during (a) unidirectional rolling at room temperature, (b) unidirectional rolling at cryogenic temperature, (c) cross-rolling at room temperature, and (d) cross-rolling at cryogenic temperature. For comparison purposes, several ideal rolling orientations are superimposed on the ODFs.

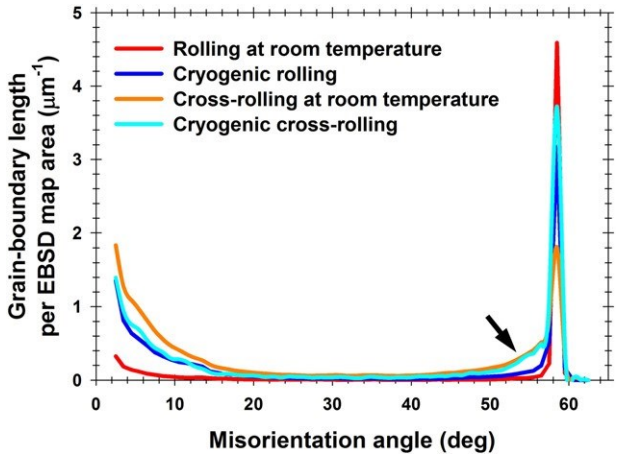

Fig. 10. Effect of cryogenic temperature and change of rolling direction on misorientation angle distribution for twinned areas.

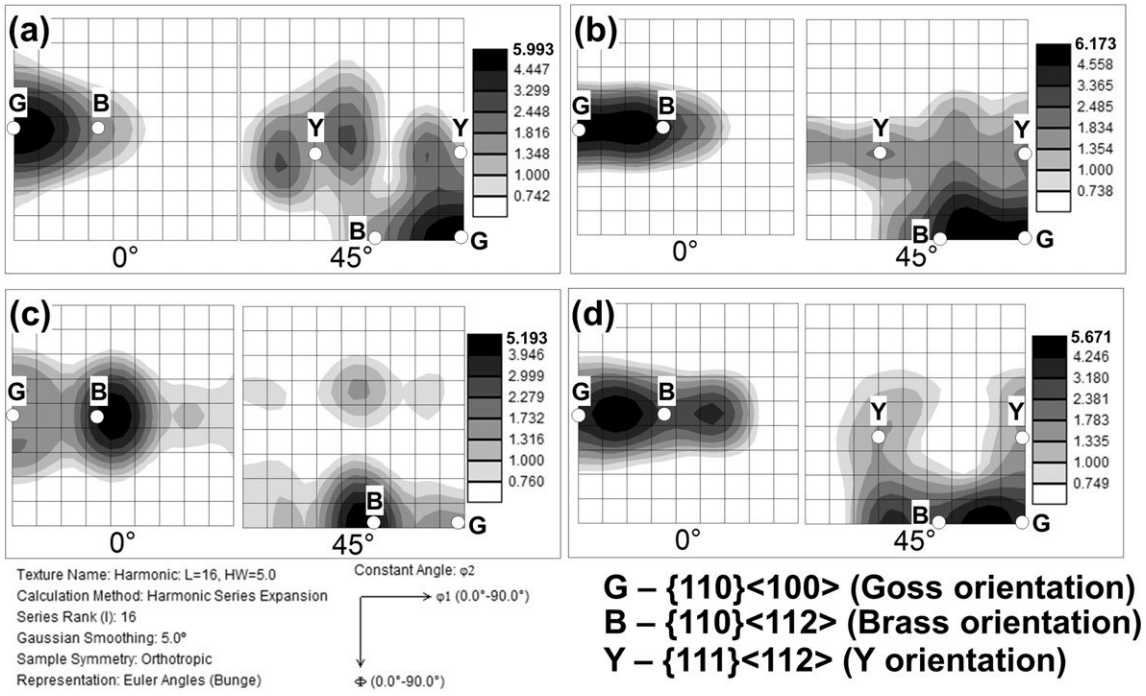

Fig. 11. φ2 = 0° and φ2 = 45° sections of ODFs for shear bands in the material which was (a) unidirectionally rolled at room temperature, (b) unidirectionally rolled at cryogenic temperature, (c) cross-rolled at room temperature, and (d) cross-rolled at cryogenic temperature. For comparison purposes, several ideal rolling orientations are superimposed on the ODFs.

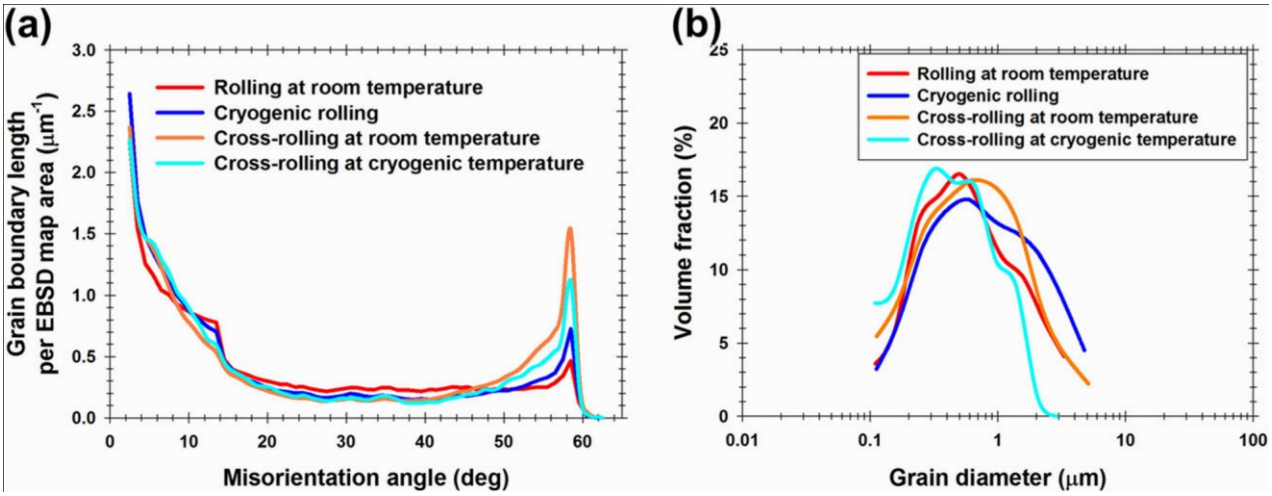

Fig. 12. Effect of cryogenic temperature and change in rolling direction on (a) misorientation-angle distribution and (b) grain-size distribution for shear-band regions.